Nuclear Inst. and Methods in Physics Research, B 412 (2017) 198–206

Contents lists available at ScienceDirect

Nuclear Inst. and Methods in Physics Research B

journal homepage: www.elsevier.com/locate/nimb

The effect of crystal size on tunneling phenomena in luminescent nanodosimetric materials

Vasilis Pagonis*, Shannon Bernier, Francisco Marques dos Santos Vieira, Shane Steele

Physics Department, McDaniel College, Westminster, MD 21157, USA

ARTICLE INFO

Keywords:
Monte Carlo model
Luminescence
Quantum tunneling
Nanocrystal

ABSTRACT

The study of luminescence signals from nanodosimetric materials is an active research area, due to the many possible practical applications of such materials. In several of these materials it has been shown that quantum tunneling is a dominant mechanism for recombination processes associated with luminescence phenomena. This paper examines the effect of crystal size on quantum tunneling phenomena in nanocrystals, based on the assumption of a random distribution of electrons and positive ions. The behavior of such random distributions is determined by three characteristic lengths: the radius of the crystal R, the tunneling length a, and the initial average distance $\langle d \rangle$ between electrons and positive ions (which is directly related to the density of charges in the material). Two different cases are examined, depending on the relative concentrations of electrons and ions. In the first case the concentration of electrons is assumed to be much smaller than the concentration of positive ions. Examination of a previously derived analytical equation demonstrates two different types of crystal size effects. When the tunneling length a is much smaller than both R and $\langle d \rangle$, the analytical equations show that smaller crystals exhibit a faster tunneling recombination rate. However, when the tunneling length a is of the same order of magnitude as both R and $\langle d \rangle$, the opposite effect is observed, with smaller crystals exhibiting a slower tunneling recombination rate. As the crystal size increases, the rate of tunneling in both cases reaches the limit expected for bulk materials. In the second case we examine the situation where the concentrations of electrons and positive ions are equal at all times. In this situation there is no analytical equation available to describe the process, and the crystal size effects are simulated by using Monte Carlo (MC) techniques. The two opposite behaviors as a function of the crystal size are also observed in these MC simulations. The effect of sample temperature is also studied by extending the MC simulations to include thermal characteristics of the defects. The relevance of the simulated results for luminescence dosimetry is discussed.

1. Introduction

The study of luminescence signals from nanodosimetric materials is an active research area, due to the many possible practical applications of such materials. In several of these materials it has been shown that quantum tunneling is a dominant mechanism for recombination processes associated with luminescence phenomena [1–19]. There are two major areas of applied research which provide the motivation for developing models to describe the properties of such nanodosimetric materials.

The first broad applied research area is in luminescence dosimetry and luminescence dating. From a dosimetry point of view, it is important to understand the tunneling mechanisms and the associated luminescence signals, with a view towards improving dosimetry and dating techniques. Quantum mechanical tunneling and the associated phenomena of "anomalous fading" and "long afterglow" of luminescence signals are now well established as dominant mechanisms in feldspars, apatites, rare earth doped materials and other important luminescent dosimetric materials See for example the recent review paper [2].

The second major experimental thrust for developing such models is for luminescence nanomaterials which find practical applications, and which consist of nanoclusters with a very small number of atoms. The synthesis and characterization of such nanodosimetric materials has become an increasingly active research area, and it has been shown that their physical properties can be different from those of similar conventional microcrystalline phosphors [1–5].

Monte Carlo simulations are often used to describe the charge creation/trapping and recombination processes in luminescent and/or dosimetric materials. Several types of simulations exist in the literature, based on either delocalized transitions involving the energy bands, or on transitions between localized states [6–10]. Larsen et al. [10]

* Corresponding author.
E-mail address: vpagonis@mcdaniel.edu (V. Pagonis).

http://dx.doi.org/10.1016/j.nimb.2017.09.016
Received 4 September 2017; Received in revised form 14 September 2017; Accepted 14 September 2017
Available online 30 September 2017
0168-583X/

presented a numerical Monte Carlo model that simulated the processes of charge loss, charge creation and charge recombination in feldspar, by assuming that the number density of electrons and holes are equal at all times. The focus of their study was to reproduce the experimentally observed values of the well-known g-factor describing anomalous fading effects. These authors were not able to get reliable results for bulk crystals, and obtained good agreement with experiment only when they assumed that the material consisted of small nanocrystals, and that charge carriers were allowed to recombine only within these smaller volumes. In parallel to this Monte Carlo modeling effort, several recent papers have developed approximate analytical equations for both the dose response of feldspars in nature, as well as for the loss of charge in these materials over geological times, due to both ground state and excited state tunneling phenomena [13,14]. Recently Pagonis and Kulp [17] presented a modified quantitative version of the model by Larsen et al. [10], in which the number density of positive ions far exceeds that of electrons. These authors were able to produce quantitative agreement of the Monte Carlo model with experimental data, by simulating the processes of charge loss and charge creation by irradiation in nature. In recent relevant work, Pagonis et al. [21] developed analytical equations for the loss of charge due to tunneling for arbitrary relative concentrations of electrons and positive ions in a solid. These analytical solutions compared well with the results of Monte Carlo simulations carried out in a random distribution of electrons and positive ions.

This paper examines the effect of crystal size on tunneling phenomena in nanocrystals, based on the assumption of a random distribution of electrons and positive ions. In the first part of the paper we consider the analytical equation derived by Tachiya and Mozumder [20], which describes the electrons survival probability in a finite random spherical distribution of electrons and scavengers of radius R. The analytical equation is valid when the concentration of positive ions far exceeds that of electrons in the system, and therefore the concentration of positive ions can be considered to stay almost constant during the tunneling process.

In the second part of the paper we examine the situation where the concentrations of electrons and positive ions are *equal* at all times during the recombination process. In this situation there is no analytical equation available to describe the process for different crystal sizes, and the crystal size effects are simulated by using Monte Carlo techniques. The advantage of the Monte Carlo techniques is that they can be extended easily to include additional physical phenomena in these small crystals, and they also provide a microscopic point of view of the luminescence process.

The purpose of the present paper is to examine tunneling recombination, with special emphasis on the effect of crystal sizes. The specific goals of the paper are:

(a) To use the previously derived analytical equation by Tachiya and Mozumder [20], in order to study the effect of crystal size on the tunneling process.
(b) To study crystal size effects by Monte Carlo simulations, for cases in which no analytical expression is available.
(c) To study by Monte Carlo simulation the effect of temperature on the rate of tunneling in crystals of different sizes.

2. The analytical equation of Tachiya and Mozumder [20]

In this section we consider crystal size effects, based on analytical equations derived by Tachiya and Mozumder [20]. These authors considered the decay of trapped electrons in glassy media in the presence of N scavengers, within the context of chemical kinetics. In the rest of this paper, we will denote the scavenger density by ρ and the tunneling frequency by s, while Tachiya and Mozumder [20] used the symbols c, ν correspondingly. In addition, the original term of "scavengers" will be referred to in this paper as "positive ions", in order to be consistent with the terms used in the recent work by Pagonis et al. [21].

When the concentration of positive ions ρ far exceeds the concentration of electrons in the system, then ρ can be considered to stay almost constant during the tunneling process.

In order to maintain charge neutrality in this system of constant ρ, it is assumed that there is a large number of additional filled electron traps in the system, which do not participate in the tunneling process. This is perhaps a very common situation in many dosimetric materials, in which several different types of electron traps are present. It is also noted that in Ref. [17] the terms "donors and acceptors" were used, instead of "electrons and positive ions" used in this paper. From the point of view of tunneling, there is no physical difference between these situations in the model, except perhaps in the values of the parameters in the model. The present model also does not consider the possibility that these charge carriers are mobile in the crystal before recombination.

By assuming that an electron can tunnel to any of the positive ions in a completely random spherical distribution of charges, these authors evaluated the probability $P(t)$ that an electron will survive at time t as:

$$P(t) = \exp\left[-t\sum_{i=1}^{N} k(r_i)\right], \tag{1}$$

where $k(r_i)$ is the rate constant for electron tunneling to a positive ion located at a distance r_i. The total electron survival probability $P(t)$ is then evaluated as the statistical average of this equation over all possible arrangements of ions around the electrons, leading to their Eq. (4):

$$P(t) = \left[\frac{1}{V}\int_V \exp[-tk(r)]dV\right]^{\rho V}, \tag{2}$$

where $V = 4/3\pi R^3$ is the volume of the spherical distribution, and the quantum tunneling rate $k(r)$ is given by:

$$k(r) = s\exp(-r/a) \tag{3}$$

where a is the attenuation length of the wavefunction, and s is the vibrational frequency in the trap. Eq. (3) shows that the quantum tunneling rate $k(r)$ depends exponentially on the distance r between electrons and ions. The effective range of any exponential function is equivalent to 5 decay constants, since the value of exponential functions drops to ~1% beyond this range. In the case of Eq. (3), the effective range of the tunneling process can then be taken as 5 tunneling lengths, and this defines an effective tunneling length $L_{eff} = 5a$.

Eq. (2) can also be written in terms of the radius R:

$$P(t) = \left[\frac{1}{(4/3\pi R^3)}\int_0^R \exp[-tk(r)]4\pi r^2 dr\right]^{\rho(4/3\pi R^3)}, \tag{4}$$

Eq. (4) can be integrated numerically for specific numerical values of ρ (in positive ions per m^3), R (m), a (m), s (s^{-1}) . This numerical calculation allows us to study the effect of finite crystal size on the tunneling recombination, as a function of time. As discussed recently in Pagonis et al. [21], it is convenient to present the results of the calculations in terms of the reduced time $t' = st$, instead of the actual time parameter t. The frequency parameter s essentially acts as a time scaling factor in the model, and does not otherwise affect the results presented here.In the limit of bulk crystals $R \to \infty$, Tachiya and Mozumder [20] showed that Eq. (4) has the following analytical expression:

$$P(t) = \exp\left[-\rho\left(\frac{4}{3}\pi a^3\right)g(st)\right], \tag{5a}$$

with

$$g(st) = \ln(st)^3 + 1.7316\ln(st)^2 + 5.9343\ln(st) + 5.4449. \tag{5b}$$

It must be noted that Eq. (4) was derived by Tachiya and Mozumder by using completely general considerations, and does not assume any specific type of interaction between electrons and positive ions. For example, derivation of Eq. (4) is *not* based on the commonly used assumption of nearest neighbor NN) interactions [13,14]. The NN

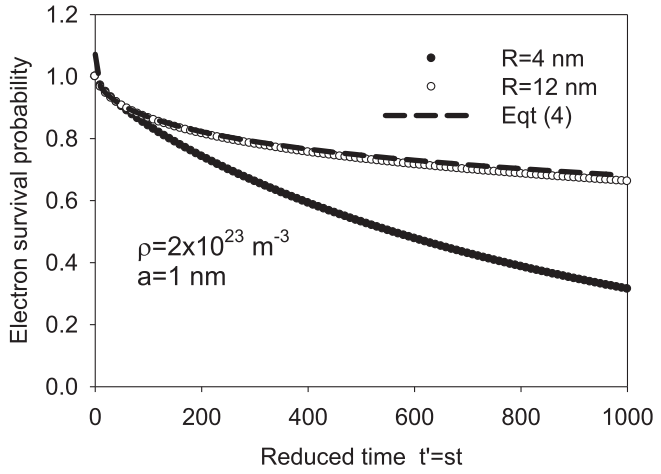

Fig. 1. The results of numerically integrating Eq. (4) for a constant ion density $\rho = 2 \times 10^{23}\,m^{-3}$, tunneling length $a = 1$ nm, and for two radii $R = 4$ nm and $R = 15$ nm. The electron survival probability $P(t)$ depends on the size of the nanocrystal R. The dashed line indicates the limit described by the analytical Eq. (5), which is applicable for bulk crystals ($R \rightarrow \infty$).

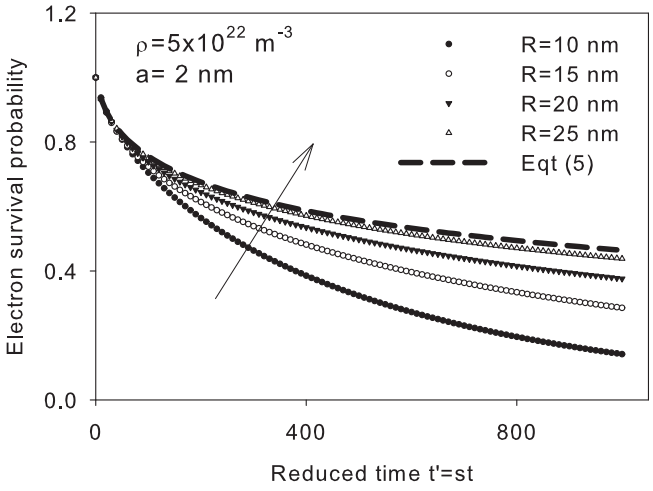

Fig. 2. The results of integrating Eq. (4) numerically for a positive ion density $\rho = 5 \times 10^{22}\,m^{-3}$, tunneling length $a = 2$ nm, and for crystal sizes $R = 10$–25 nm. As the size of the nanocrystal R is increased in the direction of the arrow, the electron survival probability increases as well, and the tunneling process becomes slower. The dashed line shows the limit described by the analytical Eq. (5).

approximation is discussed further in the section on Monte Carlo simulations.Fig. 1 shows the results of integrating Eq. (4) numerically for a constant ion density $\rho = 2 \times 10^{23}\,m^{-3}$, tunneling length $a = 1$ nm, and for two values of the radius $R = 4$ nm and $R = 15$ nm. Fig. 1 shows that the electron survival probability $P(t)$ depends on the size of the nanocrystal R. The dashed line in Fig. 1 shows the limit described by the analytical Eq. (5), which is applicable for bulk crystals ($R \rightarrow \infty$). A more detailed study of this crystal size effect is given in the next section.

In this paper we are interested mainly in the behavior of Eq. (4) as a function of the radius R, while keeping the variables ρ, a, s fixed. The mathematical dependence of the survival probability $P(t)$ on the radius R in Eq. (4) is non-trivial, and is determined by two opposite mathematical behaviors. As the radius R increases, the value of the integral of the positive function in Eq. (4) increases as well. However, this integral is also divided by the volume $V = 4/3\pi R^3$, so an increase in R would also lead to a decrease in $P(t)$. Similarly, as the radius R increases, the exponent $\rho V = \rho(4/3\pi R^3)$ also increases in Eq. (4), leading to a *decrease* of the survival probability $P(t)$, since the quantity inside the square brackets is a probability with a value less than 1. It is concluded that the function $P(t)$ depends on the radius R in a complex mathematical manner, and one can expect different types of behaviors of the function $P(t)$, depending on the numerical values of the parameters ρ, a, R.

From a physical point of view, spherical crystals with random charge distributions are characterized by three lengths:

- The radius of the crystal R
- The effective tunneling length $L_{eff} = 5a$ (discussed above)
- The average distance $\langle d \rangle = 0.542\rho^{-1/3}$ in the distribution of nearest neighbors (see Eq. (20) in Ref. [21], and also the discussion in Section 4.1 of this paper).

One would expect that the behavior of the function $P(t)$ in Eq. (4) will depend on the relative values of these 3 characteristic lengths. For a detailed discussion of the importance of characteristic lengths in the context of tunneling phenomena in chemical physics, the reader is referred to the book by Gol'danskii et al. [22].

The next section presents numerical results based on Eq. (4). It is interesting to note that while this equation has been available for more than 40 years in the literature, to the best of our knowledge it has not been used previously to describe crystal size effects, as in this paper.

3. Numerical results based on Eq. (4)

In the numerical example of Eq. (4) presented in Fig. 2, the tunneling length $a = 2 \times 10^{-9}\ m = 2$ nm is chosen to be much smaller than the radius of the sphere R, which is chosen in the range $R = 10$–25 nm. The numerical value of the density of positive ions is chosen as $\rho = 5 \times 10^{22}$ ions/m^{-3}, so that the initial average distance $\langle d \rangle = 0.542\rho^{-1/3} = 11.6$ nm is about the same as the effective tunneling length $L_{eff} = 5a = 10$ nm.Fig. 2 shows the results of integrating Eq. (4) numerically for a constant ion density $\rho = 5 \times 10^{22}\,m^{-3}$, constant tunneling length $a = 2$ nm, and for the range of values $R = 10$–25 nm. This figure shows that as the size of the nanocrystal R is increased in the direction of the arrow, the electron survival probability increases as well, and the tunneling process becomes slower. The dashed line in Fig. 2 shows the limit described by the analytical Eq. (5), which is applicable for bulk crystals ($R \rightarrow \infty$). As discussed in Tachiya and Mozumder [20], one might expect that the electron survival probability $P(T)$ reaches a finite limit very quickly for large crystals, and their statement is found to be in agreement with the behavior shown in Fig. 2. Further increase of the radius R does not change the curves shown the Fig. 2.

This type of crystal size effect depends also very strongly on the charge density ρ. Fig. 3a shows the same simulation as in Fig. 2 by keeping all parameters the same, except using a much higher density $\rho = 10^{24}\,m^{-3}$. Clearly the crystal size effect becomes much weaker, with all curves in the range $R = 10$–25 nm now practically coinciding. This is because the average distance $\langle d \rangle = 0.542\rho^{-1/3} = 5.8$ nm is now much smaller (because of the higher density), and the tunneling behavior in this range $R = 10$–25 nm of crystal sizes is the same as for bulk crystals. Fig. 3b shows the same simulation as Fig. 3a, but for much smaller crystals in the range $R = 4$–10 nm. Interestingly, Fig. 3b shows the exact opposite behavior than in Fig. 2. As the size of the nanocrystal R is increased in the direction of the arrow, the electron survival probability *decreases*, and the tunneling process becomes faster in the range $R = 4$–10 nm.

The results of Figs. 2 and 3 show clearly that the crystal size effects depend on all three parameters ρ, a, R in a rather complex manner.

Also of interest is the behavior of the tunneling process when the effective tunneling length L_{eff} is of the same order of magnitude as, or larger than the radius R of the nanocrystal. Fig. 4 shows the results of integrating Eq. (4) for a constant density $\rho = 5 \times 10^{22}\,m^{-3}$, $a = 10$ nm, and for a radius in the range $R = 15$–30 nm. The tunneling

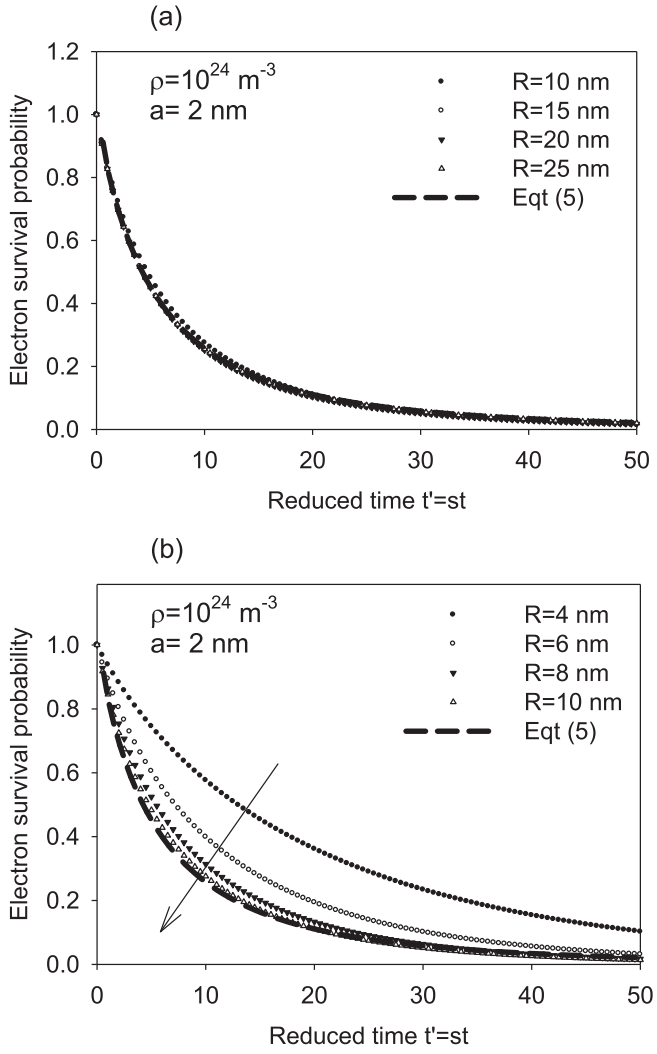

Fig. 3. (a) The same simulation as in Fig. 2, using a much higher density $\rho = 10^{24}\,m^{-3}$. The crystal size effect becomes much weaker, with all curves in the range R = 10–25 nm now practically coinciding. (b) The same simulation as (a), but for much smaller crystals in the range R = 4–10 nm. Notice that the behavior in Fig. 3b is the exact *opposite* behavior than in Fig. 2, with the tunneling process becoming faster as the size of the nanocrystal R is increased in the direction of the arrow.

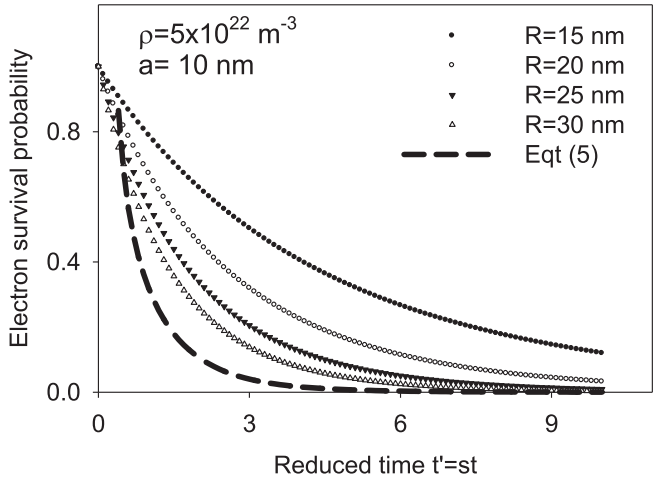

Fig. 4. The results of integrating Eq. (4) for a constant density $\rho = 5 \times 10^{22}\,m^{-3}$, a = 10 nm, and for a radius in the range R = 15–30 nm. The tunneling length a = 10 nm in this calculation is chosen 5 times larger than in Fig. 2. Notice that the behavior of $P(t)$ is similar to the behavior in Fig. 3b.

length a = 10 nm in this calculation is chosen 5 times larger than in Fig. 2, so that the effective tunneling length $L_{eff} = 5a$ = 50 nm is larger than the radius R = 15–30 nm.

Fig. 4 shows that the behavior of $P(t)$ is now similar to the behavior in Fig. 3b. As the size of the sphere R increases in the direction of the arrow, the survival probability *decreases*, and once more reaches the bulk crystal limiting value shown by the dotted line.

The results presented in this section are based on the analytical Eq. (4), whose main physical assumption is that the concentration of positive ions is much larger than the concentration of electrons, so that the system is characterized by the nearly constant density of positive ions ρ.

In the next section we consider the possibility that the system consists of an *equal* number of electrons and positive ions at all times. In this case an analytical equation similar to (4) does not exist in the literature (to the best of our knowledge), so it is necessary to use Monte Carlo methods to simulate the tunneling process.

4. Monte Carlo simulations of tunneling phenomena in small nanocrystals with equal concentrations of electrons and positive ions

Monte Carlo simulations of tunneling in a random distribution of electrons and positive ions were described in detail in Pagonis and Kulp [17]. These authors simulated rather large crystals in the range R = 100–1000 nm and found their results to be independent of the crystal size. In this paper the same simulation method is applied to much smaller nanocrystals in the range R = 50–200 nm. Section 4.1 examines the factors which affect the shape of the electron survival probability curve $P(t)$, with emphasis on the time evolution of the NN distribution of electron-ion distances. Section 4.2 presents two different examples of simulations, in which the crystal size affects the tunneling rate. Finally Section 4.3 simulates the effect of the sample temperature on the tunneling process, for small crystals.

4.1. The shape of the electron survival probability curve P(t)

The possible effects of the size of nanocrystals on tunneling phenomena were previously considered by Larsen et al. [10], who considered small cubic sub-volumes with sides d = 4–100 nm. Charge carriers in their model were only allowed to recombine within these nanocrystals. Larsen et al. [10] did not attempt to analyze the complete shape of the electron survival curves $P(t)$, but were instead more interested in the linear part of these curves to obtain the so called *g-factor*, which is of interest in luminescence dating. They considered a three-dimensional cube with volume V containing an equal number of electrons and positive charges, with tunneling taking place only to nearest neighbors. The charges are independently and randomly positioned in the volume of the box, and the *initial* number density of positive ions/electrons per unit volume is calculated by $\rho_o = n_o/V\,(m^{-3})$ where n_o is the *initial* number of electrons and positive ions in this volume.

The present work considers a *spherical* volume instead of a cube, with equal initial concentrations of electrons and positive ions n_o, as shown in Fig. 5. One possible algorithm for efficiently generating such random distributions of charges is given in Ref. [23]. The recombination of trapped charge is assumed to take place by quantum mechanical tunneling with a lifetime τ_{FADING} given by:

$$\tau_{FADING}(r) = 1/k(r) = (1/s)\exp(r/a) \quad (6)$$

where $k(r)$ was defined previously in Eq. (3). As discussed in Pagonis et al. [21], typical values of the tunneling length are a = 1–10 nm, while the values of the tunneling frequency s can vary over many orders of magnitude.

During the simulation each of the remaining electrons $n(t)$ in the spherical volume is examined, and the nearest neighbor distances r_{MIN} are calculated. The Monte Carlo algorithm generates $i = 1 \ldots n(t)$ possible random fading times t^i_{FADING} which are given by:

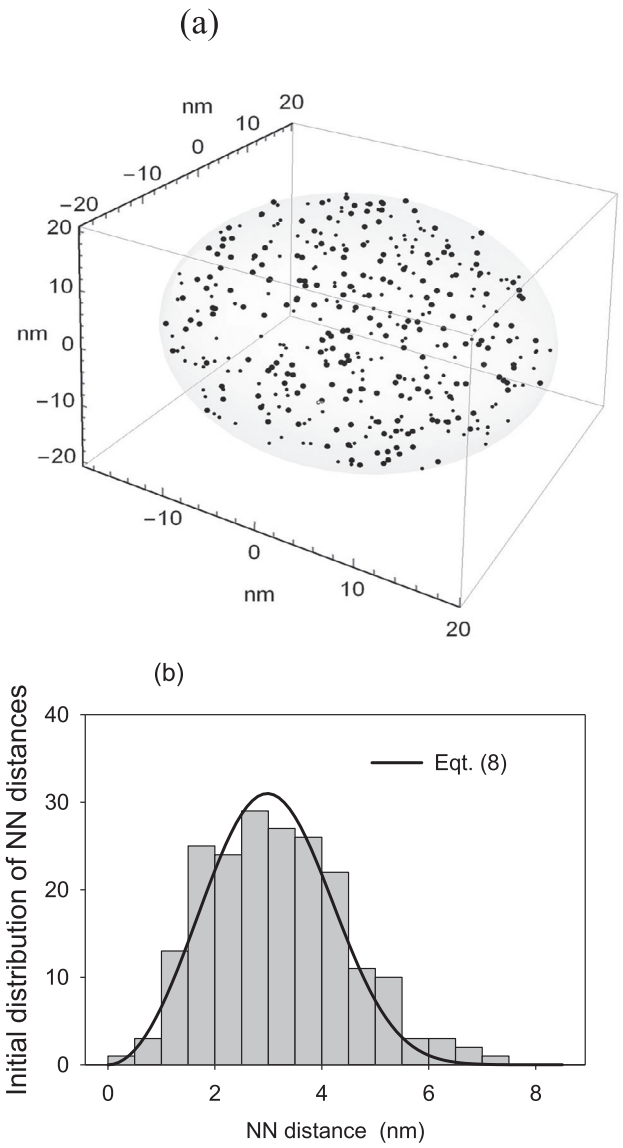

Fig. 5. (a) A random spherical distribution of $N = 200$ electrons (small dots) and $N = 200$ positive ions (large dots) in a sphere with radius $R = 20$ nm, and with a charge number density $\rho = 6\times10^{24}$ m^{-3}. (b) The distribution of nearest neighbor distances for the sphere in (a). The solid line represents the analytical Eq. (6), which applies to large crystals with a macroscopic charge density ρ.

$$t^{i}_{FADING} = -(1/s)\exp(r_{MIN}/a)\ln(1-P_i) i = 1...n(t) \quad (7)$$

where P_i is a random number between 0 and 1, representing the probability of recombination for each surviving electron. Close-by pairs are more likely to recombine first, and further away pairs are likely to recombine later. Only the event corresponding to the shortest of all the possible times in Eq. (7) happens, i.e. the electron-ion pair corresponding to this shortest time is allowed to recombine. After this pair is removed from the system in the simulation, the distances between each electron and the positive ions are re-evaluated, and the minimum t^{i}_{FADING} time is used to update the total time elapsed from the beginning of the simulation. This process is repeated until there are no more electrons left in the system. The simulation is coded in the commercial software package *Mathematica*, and the distances of each electron from all positive ions is calculated by using the native *Mathematica* commands *Nearest* and *EuclideanDistance*. Typical running times are a few minutes for a simulation consisting of 200 electrons and 200 positive ions.

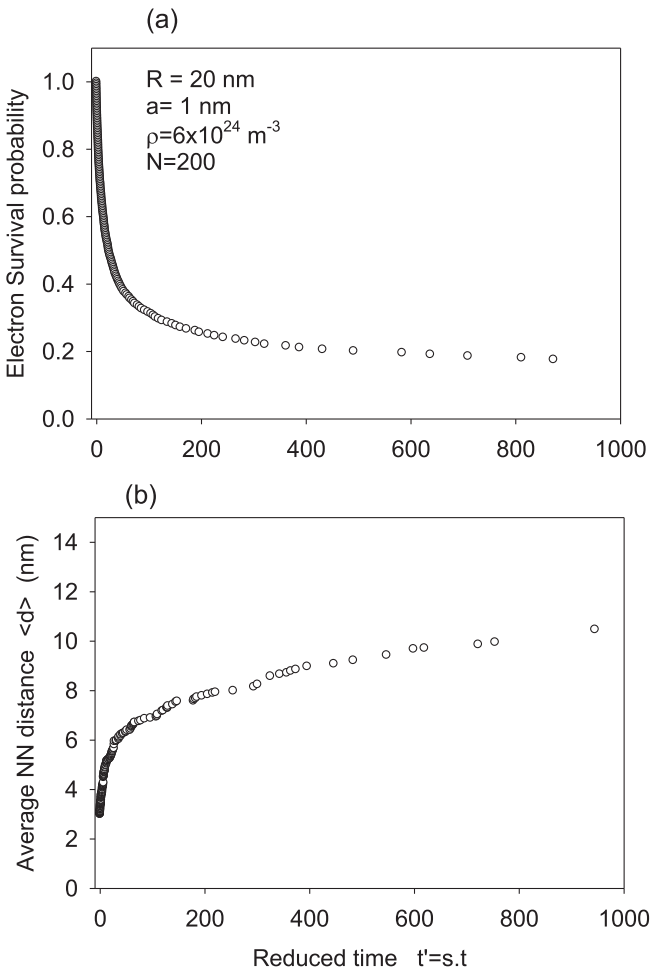

Fig. 6. (a) Typical Monte Carlo results, showing the average of 100 Monte Carlo variants of the sphere with the parameters used for the simulation given in the text. Two distinct regions are seen in the curve, a fast decay region i for small values of the reduced time parameter $t' = 0$–40, and a slower decay region for large values of $t' > 40$. (b) The average NN distance between the charges inside the sphere at different times, during the simulation shown in (a). In the slow decay region with $t' = 0$–40, the average distance between charges increases quickly in the range 3–6 nm, while in the large times region $t' > 40$ the average distance increases slowly in the range ~6–10 nm.

The program keeps track of the remaining number of electrons $n(t)$ in the system, and calculates the electron survival probability $P(t) = n(t)/n_o$ where n_o is the initial number of electrons and ions inside the sphere. For a *bulk* crystal with a constant charge density ρ and a large but finite radius R, the distribution of NN distances r is given by the well-known analytical normalized expression [17,21]:

$$g(r) = 4\pi\rho r^2\exp[-4\pi\rho r^3] \quad (8)$$

By taking the derivative in this equation and setting it equal to zero, the maximum of the nearly symmetric distribution $g(r)$ of NN distances is found to occur at an average distance $\langle d\rangle = 0.542\rho^{-1/3}$, and the maximum height of this normalized distribution is equal to $1.895\rho^{1/3}$. Fig. 5a shows a random spherical distribution of $N = 200$ electrons (small dots) and $N = 200$ positive ions (large dots) in a sphere with radius $R = 20$ nm and with a charge number density $\rho = 6 \times 10^{24}$ m^{-3}. Fig. 5b shows the distribution of nearest neighbor distances for the sphere in Fig. 5a, in the form of a histogram. The solid

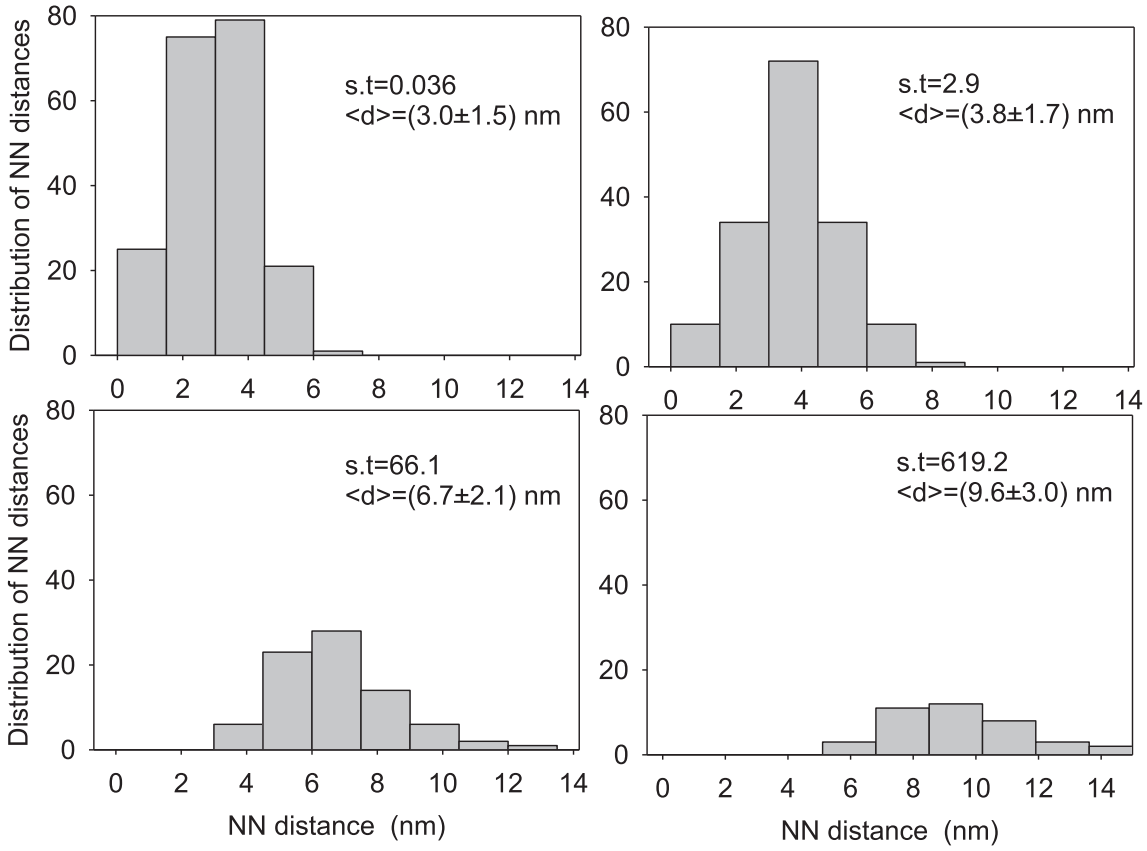

Fig. 7. The time evolution of the NN distances inside the sphere at different times during the tunneling process. The distribution progressively shifts towards higher distances, because close-by pairs recombine first, and the average distances increase with time. This is the "redistribution of distances" with time also reported by Larsen et al. [10].

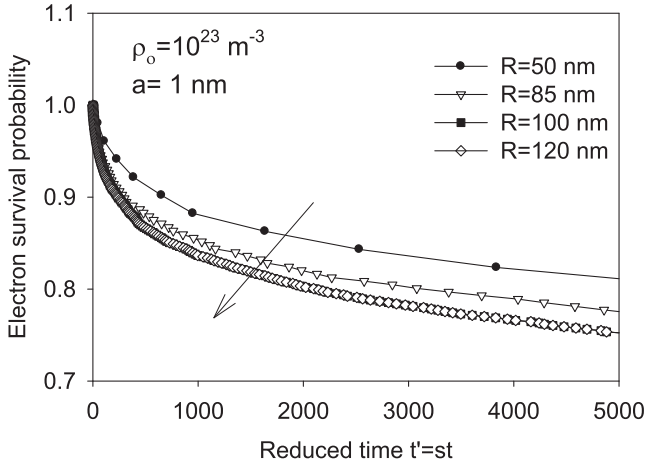

Fig. 8. Monte Carlo simulation when the tunneling length $a = 1$ nm is chosen to be much smaller than the radius of the spheres $R = 50$–120 nm. The initial number density of electrons and ions is kept constant at $\rho_o = 10^{23}$ pairs/m^3. As the radius of the crystal is *increased* in the direction of the arrow, the tunneling rate *increases* as well, and it reaches a limit for crystal sizes larger than $R \sim 100$ nm. Notice that this behavior is very similar to the simulations shown in Fig. 4.

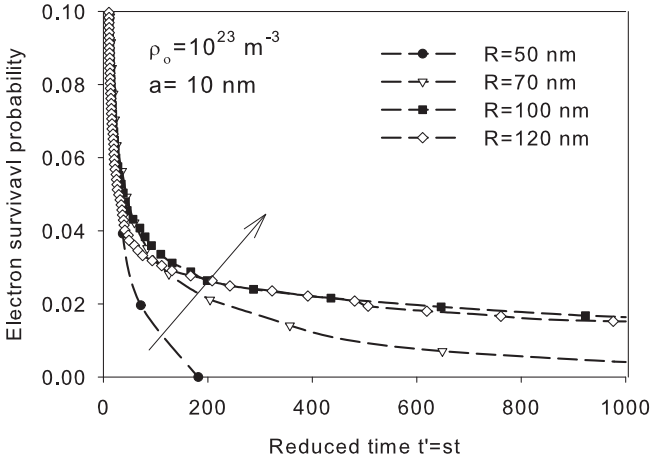

Fig. 9. The same simulation as in Fig. 8, but the tunneling length is increased from $a = 1$ nm to $a = 10$ nm. As the size of the sphere R increases in the direction of the arrow, the rate of tunneling *decreases*, in an opposite direction to the effect shown in Fig. 7.

line represents the analytical Eq. (8), which applies to large crystals with a macroscopic number density ρ. Good agreement can be seen between analytical Eq. (8) and the discrete histogram distribution in Fig. 5b.

Fig. 6a shows a typical example of the survival probability $P(t)$ as a function of the dimensionless reduced time $t' = st$. The data in Fig. 6a represents the average of 100 Monte Carlo variants of the sphere and the parameters used for the simulation are the initial charge density $\rho_o = 6 \times 10^{24}\,\mathrm{m}^{-3}$, tunneling length $\alpha = 1$ nm, $n_o = 200$ and $R = 20$ nm.

There are clearly two distinct regions in the curve of Fig. 6a. A fast decay region is seen for small values of the parameter $t' = 0$–40, and a slower decay region corresponding to large values of $t' > 40$. The

existence of these "fast" and "slow" time regions is of possible interest to experimental work on luminescent materials. For example, experimental work on luminescence signals from feldspars and apatites has shown the existence of both "fast" and "slow" tunneling components see for example Refs. [15,16,18] for a detailed analysis of thermoluminescence TL) and optically stimulated luminescence OSL) signals from several feldspars, and Ref. [12] for a case study of CW-IRSL signals from a variety of samples). Furthermore, the region of slower tunneling rate seen in Fig. 6a, is similar to the experimentally observed long term tunneling afterglow signal in a variety of luminescent materials Ref. [1] and references therein).

Fig. 6b shows the average NN distance between the charges inside the sphere at different times, during the simulation shown in Fig. 6a. In the slow decay region with $t' = 0$–40, the average distance between charges increases rather quickly from ~3 nm to ~6 nm, while in the large times region $t' > 40$ the average distance increases slowly from ~6 nm up to ~10 nm.

Fig. 7 shows the time evolution of the NN distances inside the sphere at different times during the tunneling process, in histogram form. It is clear by comparison of the histograms in Fig. 7, that the shape of the distribution of distances changes with time, and that the distribution progressively shifts towards higher distances. This makes physical sense, since one would expect that close-by pairs will recombine first, and this leads to the increase of the average distances shown in Fig.6b, as time progresses. This "redistribution of distances" with time was also reported in the simulations of Larsen et al. Ref. [10], their Fig. 3).

In conclusion, Figs. 6b and 7 provide a physical explanation for the existence of the two distinct fast and slow time regions in the tunneling process. In the fast decay region $t' < 40$ the distribution of distances remains close to symmetric, and the average distance between electrons and positive ions increases quickly with time. In the slow decay region $t' > 40$, close-by charges have already recombined, and the average distance increases at a much slower rate, since only far away pairs remain at later times inside the sphere.

In the next subsection we examine the effect of crystal size R on these Monte Carlo simulations.

4.2. The effect of crystal size R on the tunneling rate

In the Monte Carlo simulation presented in Fig. 8, the tunneling length $a = 1$ nm is chosen to be much smaller than the radius of the spheres, which is chosen in the range $R = 50$–120 nm. The initial number density of electrons and ions is chosen as $\rho_o = 10^{23}$ pairs/m^3, so that the initial average distance is $\langle d \rangle = 0.542\rho^{-1/3} = 11.6$ nm. Fig. 8 shows the results of the Monte Carlo simulations, with the initial number density ρ_o kept constant. As the radius of the crystal is *increased* in the direction of the arrow, the tunneling rate *increases* as well, and it reaches a limit for crystal sizes larger than $R \sim 100$ nm. No further changes are observed in the curves for larger crystal sizes. This behavior of $P(t)$ for different R values is very similar to the simulations shown in Fig. 4. The important difference between these two figures is that Fig. 4 is based on a *constant* concentration of ions ρ and on the analytical Eq. (4), while Fig. 8 is based on a *variable* concentration $\rho(t)$ and on Monte Carlo methods.

Fig. 9 shows a different behavior of the tunneling process when the tunneling length is increased from $a = 1$ nm to $a = 10$ nm, while the rest of the parameters remain the same as in Fig. 8. As the size of the sphere R increases in Fig. 9 in the direction of the arrow, the rate of tunneling *decreases*, in an opposite direction to the effect shown in Fig. 8. Finally for very large crystals the rate of tunneling increases to a limiting value, and further increase of the R value does not change the curves in the Fig. 9.

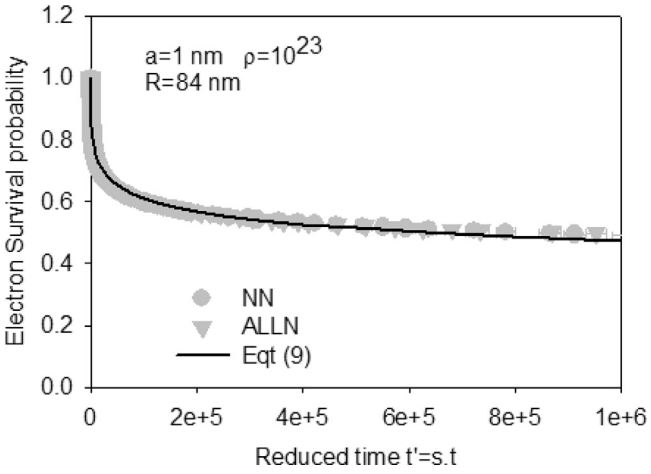

Fig. 10. Example of Monte Carlo calculations carried out by using the NN approximation (circles), and by using the all-neighbors (ALLN) approximation (triangles). The solid line indicates the analytical expression (9).

The question arises on whether the results of Figs. 8 and 9 depend on the NN approximation used during in the Monte Carlo simulations. One might expect that the NN assumption will be a good approximation in general, unless one is dealing with extremely high charge densities Ref. [22]. Fig. 10 shows an example of Monte Carlo calculations carried out by using the NN approximation (circles), and by using the all-neighbors (ALLN) approximation (triangles). The computer program was adjusted in the ALLN simulation, so that it calculates the distances from each electron to *all* possible positive charges in the sphere. The rest of the algorithm remains the same, and the parameters used are the same for both NN and ALLN simulations in Fig. 10.

The solid line indicates the following analytical expression derived recently by Pagonis et al. [21] for large crystals:

$$P(t) = 1/\{1 + (4\pi/3)n_o a^3[\ln(st)]^3\} \tag{9}$$

Good agreement is seen between the analytical expression for these large crystals, and the corresponding Monte Carlo simulations.

We have also compared the tunneling curves for a spherical and a cubic distribution of charges, using the same charge density and the same kinetic parameters. The simulations showed that the behavior of the system is the same for the cubic and spherical distributions, and therefore the results do not depend on the shape of the crystals, at least within the range of parameters used in this paper.

4.3. The effect of temperature on the crystal size effects

Larsen et al. [10] in their Monte Carlo model discussed the possibility of recombinations taking place due to either thermal or tunneling processes. They showed that in such cases the Eq. (7) in this paper must be modified as follows see Ref. [10], their Eq. (5)):

$$t^i_{RECOMBINATION} = -\left(\frac{\tau_{THERMAL}\cdot\tau_{FADING}}{\tau_{FADING} + \tau_{THERMAL}}\right)\ln(1-P_i) \quad i = 1\cdots n(t) \tag{10}$$

Where $\tau_{THERMAL} = (1/s)\exp(E/kT)$ is the thermal time constant, which is assumed to be constant and the same for all traps. This Arrhenius-type thermal time constant $\tau_{THERMAL}$ is characterized by the thermal activation energy E and the thermal frequency factor s, k is the Boltzmann constant and T is the temperature of the sample.

Fig. 11 shows Monte Carlo simulations carried out using the modified Eq. (10), with the values of $E = 1$ eV, $s = 10^{12}$ s^{-1}, initial charge density $\rho_o = 5 \times 10^{23}$ m^{-3}, $a = 1$ nm and crystal sizes $R = 34$–78 nm.

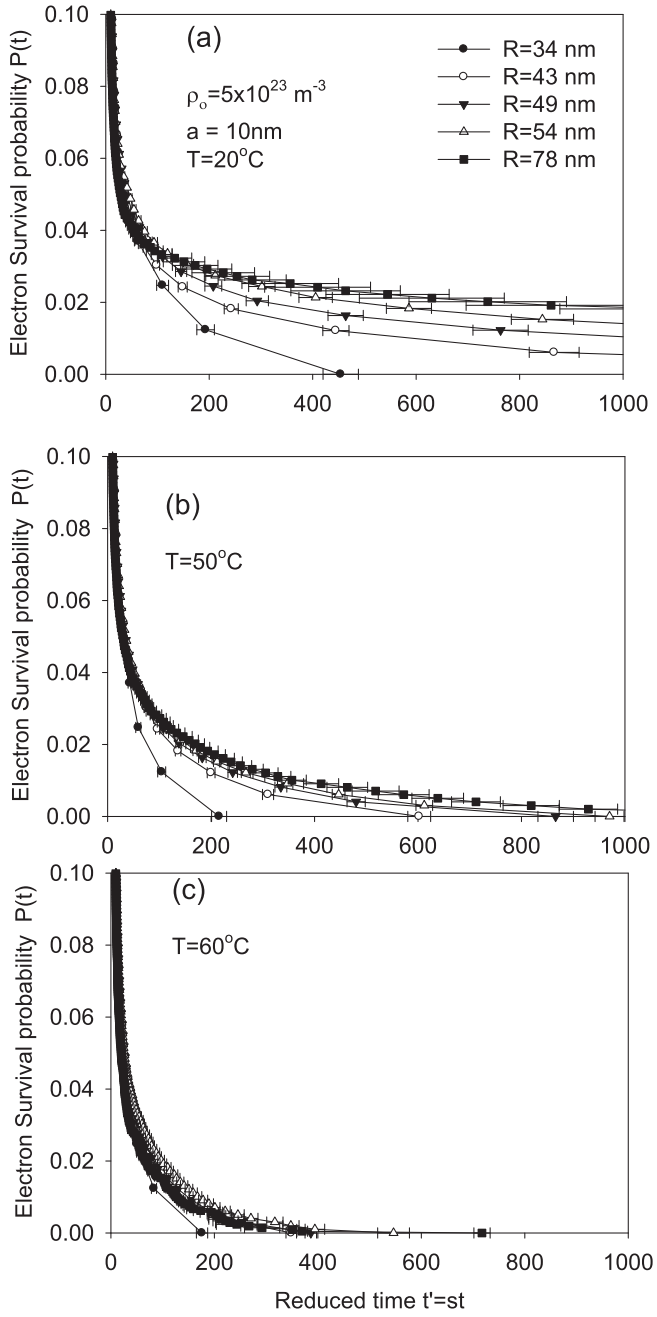

Fig. 11. Monte Carlo simulations of the effect of sample temperature on the tunneling process, using the modified Eq. (9). (a)–(c) The simulations are shown at three different sample temperatures T = 20, 50, 60 °C. As the temperature of the sample increases, recombination takes places faster and the crystal size effect shown in (a) becomes much less noticeable at higher temperatures.

The simulations are show at three different sample temperatures T = 20, 50, 60 °C.

As the temperature of the sample increases, the electron survival probability curves $P(t)$ become steeper, i.e. the recombination takes places faster. Furthermore, the curves $P(t)$ become closer together, and the crystal size effect shown in Fig. 11a becomes much less noticeable in Fig. 11c.

5. Summary and discussion

Eq. (4) previously derived by Tachiya and Mozumder [20] shows that tunneling phenomena in a spherical random distribution of charges depend on three lengths, which characterize the system. These are the radius of the nanocrystal R, the average distance $\langle d\rangle = 0.542\rho^{-1/3}$ (which depends on the charge density), and the effective tunneling length $L_{eff} = 5a$ (a = tunneling length representing the width of the wavefunction). The first two lengths R, $\langle d\rangle$ depend on the manufacturing conditions of the material, while the third length $L_{eff} = 5a$ is a physical characteristic of the material. When the concentrations of electrons and positive ions are equal at all times, one has to resort to Monte Carlo simulations, since there are no analytical equations for this case. In all situations the behavior for different crystal sizes is complex, and the rate of tunneling can either increase or decrease, as the radius R is increased.

From an experimental point of view, this rate of tunneling is directly related to the *g-factor*, which characterizes the fading of luminescence signals in feldspars, apatites and other similar materials used in dating applications [10]. The simulations in this paper show that the variation of the *g-factor* with the crystal size R depends on the relative values of the three characteristic lengths $\langle d\rangle$, R, L_{eff}. Specifically as R increases, the *g-factor* can either decrease or increase, depending on the physical properties of the material.

In recent experiments Polymeris et al. [19], submitted) found that ball milling of Durango apatite powders resulted in a decrease of the g factor for some of the luminescence signals in this material. This behavior is similar to the behaviors studied in this paper. The simulations and analytical considerations in this paper can also help researchers understand the origin and physical characteristics of the long afterglow signals reported in a variety of nanodosimetric materials.

As in previous modeling studies, this paper does not consider the effect of retrapping of charge carriers in empty traps, which is assumed to be negligible. However, we do consider the effects of thermal stability of the traps, with typical results shown in Fig. 11 for the effect of sample temperature on the electron survival curves $P(t)$. Finally, the work in this paper can easily be extended to studying the effect of crystal size on the dose response of materials, both in nature and in the laboratory [17].

Acknowledgement

This work was supported by McDaniel College as part of the summer faculty-student collaborative research initiatives.

References

[1] K.V. Eeckhout, P.F. Smet, D. Poelman, Materials 3 (2010) 2536–2566.
[2] V. Pagonis R. Chen C. Kulp G. Kitis, Radiat. Meas. Corrected Proofs: 2017 10.1016/j.radmeas.2017.01.001 (in press).
[3] N. Salah, Nanocrystalline materials for the dosimetry of heavy charged particles: a review, Radiat Phys. Chem. 80 (2011) 1–10.
[4] H.T. Sun, Y. Sakka, Sci. Technol. Adv. Mater. 15 (2014) 014205, http://dx.doi.org/10.1088/1468-6996/15/1/014205.
[5] I. Eliyahu, Y.S. Horowitz, L. Oster, S. Druzhyna, I. Mardor, Radiat. Meas. 71 (2014) 226–231.
[6] A. Mandowski, J. Świątek, Synth. Met. 109 (2000) 203–206.
[7] A. Mandowski, Radiat. Prot. Dosim. 119 (2006) 85–88.
[8] V. Pagonis, G. Kitis, Phys. Status Solidi B 249 (2012) 1590–1601.
[9] A. Mandowski, A.J.J. Bos, Radiat. Meas. 46 (2011) 1376–1379.
[10] A. Larsen, S. Greilich, M. Jain, A.S. Murray, Radiat. Meas. 44 (2009) 467.
[11] N.R.J. Poolton, R.H. Kars, J. Wallinga, A.J.J. Bos, J. Phys. Condens. Matter 21 (2009) 485505.
[12] V. Pagonis, M. Jain, K.J. Thomsen, A.S. Murray, J. Lumin. 153 (2014) 96–103.
[13] M. Jain, B. Guralnik, M.T. Andersen, J. Phys. Condens. Matter 24 (2012) 385402 (12pp).

[14] G. Kitis, V. Pagonis, J. Lumin. 137 (2013) 109–115.
[15] I.K. Sfampa, G.S. Polymeris, V. Pagonis, E. Theodosoglou, N.C. Tsirliganis, G. Kitis, Nucl. Instrum. Method Phys. Res. B 359 (2015) 89–98.
[16] G.S. Polymeris, N. Tsirliganis, Z. Loukou, G. Kitis, Phys. Status Solidi. (a) 203 (2006) 578.
[17] V. Pagonis, C. Kulp, J. Lumin. 181 (2017) 114–120.
[18] I.K. Sfampa, G.S. Polymeris, N.C. Tsirliganis, V. Pagonis, G. Kitis, Nucl. Instrum. Method Phys. Res. B 320 (2014) 57–63.
[19] G.S. Polymeris, I.K. Sfampa, M. Niora, E.C. Stefanaki, L. Malletzidou, V. Giannoulatou, V. Pagonis, G. Kitis, Radiat. Meas (2017) currently under review.
[20] M. Tachiya, A. Mozumder, Chem. Phys. Lett. 28 (1974) 87.
[21] V. Pagonis, C. Kulp, C. Chaney, M. Tachiya, J. Phys. Condens. Matter 29 (2017) 365701.
[22] V.I. Gol'danskii, L.I. Trakhtenberg, V.N. Fleurov, Tunneling Phenomena in Chemical Physics, Gordon and Breach Science publishers, New York, 1988.
[23] Weisstein, Eric W. Ball Point Picking. From MathWorld – A Wolfram Web Resource. http://mathworld.wolfram.com/BallPointPicking.html.